Nonparametric reconstruction of the dark energy equation of state from diverse data sets

Tracy Holsclaw, Ujjaini Alam, Bruno Sansó, Herbie Lee, Katrin Heitmann, Salman Habib, and David Higdon

Phys. Rev. D **84**, 083501 — Published 3 October 2011

DOI: 10.1103/PhysRevD.84.083501

LA-UR-11-01798

Nonparametric Reconstruction of the Dark Energy Equation of State from Diverse Data Sets

Tracy Holsclaw,[1] Ujjaini Alam,[2] Bruno Sansó,[1] Herbie Lee,[1]
Katrin Heitmann,[2,3] Salman Habib,[4,3] and David Higdon[5]

[1] *Department of Applied Mathematics and Statistics, University of California, Santa Cruz, CA 95064*
[2] *ISR-1, MS D466, Los Alamos National Laboratory, Los Alamos, NM 87545*
[3] *High Energy Physics Division and Mathematics and Computer Science Division, Argonne National Laboratory, Argonne, IL, 60439*
[4] *T-2, MS B285, Los Alamos National Laboratory, Los Alamos, NM 87545*
[5] *CCS-6, MS F600, Los Alamos National Laboratory, Los Alamos, NM 87545*

(Dated: August 30, 2011)

The cause of the accelerated expansion of the Universe poses one of the most fundamental questions in physics today. In the absence of a compelling theory to explain the observations, a first task is to develop a robust phenomenological approach: If the acceleration is driven by some form of dark energy, then, the phenomenology is determined by the form of the dark energy equation of state $w(z)$ as a function of redshift. A major aim of ongoing and upcoming cosmological surveys is to measure w and its evolution at high accuracy. Since $w(z)$ is not directly accessible to measurement, powerful reconstruction methods are needed to extract it reliably from observations. We have recently introduced a new reconstruction method for $w(z)$ based on Gaussian process modeling. This method can capture nontrivial $w(z)$ dependences and, most importantly, it yields controlled and unbiased error estimates. In this paper we extend the method to include a diverse set of measurements: baryon acoustic oscillations, cosmic microwave background measurements, and supernova data. We analyze currently available data sets and present the resulting constraints on $w(z)$, finding that current observations are in very good agreement with a cosmological constant. In addition we explore how well our method captures nontrivial behavior of $w(z)$ by analyzing simulated data assuming high-quality observations from future surveys. We find that the baryon acoustic oscillation measurements by themselves already lead to remarkably good reconstruction results and that the combination of different high-quality probes allows us to reconstruct $w(z)$ very reliably with small error bounds.

PACS numbers: 98.80.-k, 02.50.-r

I. INTRODUCTION

The discovery of the accelerated expansion of the Universe little more than a decade ago [1, 2] was a major surprise. Since then, many observational efforts to understand the underlying cause have been initiated, such as the recently completed WiggleZ survey [3] and the ongoing Baryon Oscillation Spectroscopic Survey (BOSS) [4]. The Dark Energy Survey (DES, https://www.darkenergysurvey.org/) is scheduled to begin in 2012 and construction of the Large Synoptic Survey Telescope (LSST) [5] is ongoing. Proposed surveys include BigBOSS [6], the Wide Field Infrared Survey Telescope (WFIRST) [7], and Euclid [8]. All these efforts focus on a set of diverse cosmological probes (supernovae, baryon acoustic oscillations, clusters of galaxies, weak lensing, etc.) to combine the best possible observations in order to help solve the puzzle of cosmic acceleration.

The two currently most popular explanations are a form of dark energy or a modification of Einstein's theory of gravity on the largest observable scales. We will focus in this paper on dark energy as the cause for the accelerated expansion. The simplest way to realize a dark energy is via a cosmological constant with a dark energy equation of state specified by $w = p/\rho = -1$. A cosmological constant, however, is not theoretically well-motivated. If we assume that the origin is due to a vacuum energy, the predicted value is incorrect at the order of 10^{60}. Therefore, a more natural realization of dark energy might be a dynamical field, similar to the inflaton that is believed to drive the very early rapid expansion of the Universe. Such a dynamical field, described for example by quintessence models [9], would lead to a non-constant dark energy equation of state parameter $w(z)$. It is therefore one of the major aims of ongoing and upcoming dark energy missions to measure $w(z)$ and its time variation with high accuracy. If $w(z)$ is modeled via a simple parametrization $w(z) = w_0 + w_a z/(1+z)$ [10, 11], current predictions for future surveys promise measurements of the constant piece at the 1% level accuracy and of the leading time variance at the 10% level. At present, the best measurements are accurate to better than 10% for a constant dark energy equation of state [12–14] and w_0 is constrained at the 20% level if a time variation parameterized by $w_0 - w_a$ is allowed. In this case, Ref. [14] finds an uncertainty in w_a of 100%, assuming a flat universe.

With the prospect of high-accuracy measurements from supernova (SN) surveys and complementary large-scale structure probes such as baryon acoustic oscilla-

tion (BAO) surveys, it is desirable to develop an accurate reconstruction method with reliable error bars that allows us to extract the dark energy equation of state from different measurements. While parametric methods have been widely employed [10, 11, 15], non-parametric techniques constitute a useful alternative [16]. Non-parametric methods are less susceptible to modeling bias as no assumptions are made regarding the functional form for $w(z)$ (for a discussion of modeling bias in parametric methods, see Ref. [17]). Of course, if the data quality is insufficient non-parametric approaches provide little additional information over that given by a simple parameterization. Even in this case, however, it is better to obtain uncertain results with larger errors than a possibly biased prediction due to the particular choice of functional form assumed for $w(z)$, without this bias being properly reflected in the error estimation.

In this paper, we discuss a recently-introduced reconstruction method based on Gaussian process (GP) modeling [18, 19]. A GP is a stochastic process in which each realization is a random draw from a multivariate Normal distribution. It is characterized by mean and covariance functions defined by a small number of parameters. Bayesian estimation methods are used to determine the parameters of the GP model together with any other physics parameters. Therefore, the final form of the GP model is informed by the data itself. The form of the covariance function is general enough to accommodate a large variety of possible outcomes for $w(z)$. The only assumptions made are mild constraints on the smoothness and continuity properties of $w(z)$. It is hard to imagine physically motivated explanations for an accelerated expansion that are inconsistent with these properties.

In Ref. [19], GP modeling was used to solve the statistical inverse problem of going from observed supernova data alone to a direct constraint on $w(z)$, resulting in an allowed 68% acceptance band around $w = -1$ with a width of roughly ± 0.2, over a redshift range of $z = 0-1.5$ – a striking illustration of the power of the method.

Our purpose here is to extend the above approach (described in detail in Ref. [18]) to include different observational probes of $w(z)$, namely supernova measurements, cosmic microwave background (CMB) observations, and BAO results. We begin with an analysis of currently available data. We find, not surprisingly, that our predictions are in good agreement with a cosmological constant. Using simulated data, we then explore the ability to extract variations of $w(z)$ away from a cosmological constant with improving accuracy and statistics of the data. The inclusion of the additional BAO and CMB measurements help greatly to improve these predictions.

The paper is organized as follows. In Section II we describe the different data sources included in our analysis, namely, supernova, CMB, and BAO measurements. In Section III we describe our GP model based reconstruction method. We carry out an analysis of currently available data in Section IV. We demonstrate that the method will allow us to extract variations in the dark energy equation of state by using simulated data in Section V. (This also allows us to study the sensitivity of extracting cosmological parameters as a function of realizations of the observed data sets, a form of cosmic variance.) Finally, we conclude in Section VI.

II. DARK ENERGY EQUATION OF STATE FROM DIVERSE DATA SETS

Type Ia supernova measurements are currently the best source of information regarding possible deviations of $w(z)$ from a constant value. In the future, BAO (and other) measurements will be strong competitors and in combination will lead to the best possible constraints on $w(z)$. The complementarity of the different probes is important to break degeneracies and decrease the overall errors. In previous work [18] we have shown that our non-parametric reconstruction method can capture even relatively sharp transitions in $w(z)$ well provided independent knowledge of Ω_m is available. Supernova data alone, however, does not provide this information and one needs a strong prior on Ω_m to obtain good results (justified by assuming the existence of complementary probes). In a more direct and complete implementation, as performed here, multiple probes can be directly included in a joint analysis. This allows us to relax our prior assumptions on Ω_m and to tighten the final constraints on the behavior of $w(z)$.

In the following, we provide a brief review of the different dark energy probes employed in this paper – supernovae, BAO, and CMB – and how to extract information about $w(z)$ from these probes. We focus in this paper on the geometric probes for $w(z)$. The GP analysis in this case is very similar for all methods – $w(z)$ is connected via two derivatives with the different distance measures. In the next section, we explain in detail how to set up a joint GP model for the three different observations.

A. Supernova Measurements

In this paper we retain the notation from our previous work [18]. For completeness, we summarize the important equations here. The luminosity distance d_L as measured by supernovae is directly connected to the expansion history of the Universe described by the Hubble parameter $H(z)$. For a spatially flat Universe, the relation is given by

$$d_L(z) = (1+z)\frac{c}{H_0}\int_0^z \frac{ds}{h(s)}, \tag{1}$$

where c is the speed of light, H_0, the current value of the Hubble parameter ($H(z) = \dot{a}/a$, where a is the scale factor and the overdot represents a derivative with respect to cosmic time), and $h(z) = H(z)/H_0$. The assumption of spatial flatness is in effect an "inflation prior",

although there do exist strong constraints on spatial flatness when CMB and BAO observations are combined (see, e.g., Ref. [20]). In principle, we can relax this assumption, but enforce it here to simplify the analysis.

Instead of $d_L(z)$, supernova data are usually specified in terms of the distance modulus μ as a function of redshift. The relation between μ and the luminosity distance is

$$\begin{aligned}\mu_B(z) = m_B - M_B &= 5\log_{10}\left(\frac{d_L(z)}{\rm Mpc}\right) + 25 \qquad (2)\\ &= 5\log_{10}\left[(1+z)\int_0^z \frac{ds}{h(s)}\right]\\ &\quad +5\log_{10}\left(\frac{c}{H_0}\frac{1}{\rm Mpc}\right) + 25,\end{aligned}$$

where we have used Eq. (1). M_B is the absolute magnitude of the object and m_B the (B-band) apparent magnitude. Writing out the expression for the reduced Hubble parameter $h(z)$ in Eq. (2) explicitly in terms of a general dark energy equation of state for a spatially flat FRW Universe, one finds:

$$\begin{aligned}h^2(z) &= \Omega_r(1+z)^4 + \Omega_m(1+z)^3 \qquad (3)\\ &\quad +(1-\Omega_r-\Omega_m)(1+z)^3\exp\left(3\int_0^z \frac{w(u)}{1+u}du\right),\end{aligned}$$

which leads to the relation,

$$\begin{aligned}\mu_B(z) &= 25 + 5\log_{10}\left(\frac{c}{H_0}\frac{1}{\rm Mpc}\right) \qquad (4)\\ &+5\log_{10}\left\{(1+z)\int_0^z ds\left[\Omega_r(1+s)^4 + \Omega_m(1+s)^3\right.\right.\\ &\left.\left. +\ (1-\Omega_r-\Omega_m)(1+s)^3\exp\left(3\int_0^s \frac{w(u)}{1+u}du\right)\right]^{-1/2}\right\}.\end{aligned}$$

While the term proportional to Ω_r (the radiation density for photons and neutrinos) is negligible at low redshift, we include it in the equations for completeness – it will become important for the CMB and BAO measurements. We use the following relation for Ω_r when CMB is added to the analysis:

$$\Omega_r(a) = \Omega_\gamma[1 + 0.227 N_{\rm eff} f(m_\nu a/T_\nu)], \qquad (5)$$

where for the standard three neutrino species, $N_{\rm eff} = 3.04$, we have

$$\frac{m_\nu a}{T_\nu} = \frac{187}{1+z}\left(\frac{\Omega_\nu h^2}{10^{-3}}\right), \qquad (6)$$

and

$$f(y) \simeq [1 + (0.3173y)^{1.83}]^{1/1.83} \qquad (7)$$

For more details see Ref. [20], specifically Eq. (26) for the expression for $f(y)$.

Note that H_0 in Eq. (4) cannot be determined from supernova measurements in the absence of an independent distance measurement. Thus H_0 can be treated as an unknown and absorbed in a re-definition of the absolute magnitude $\mathcal{M}_B = M_B - 5\log_{10} H_0 + 25$, which accounts for the combined uncertainty in the absolute calibration of the supernova data, as well as in H_0. Using this, the B-band magnitude can be expressed as $m_B = 5\log_{10} D_L(z) + \mathcal{M}_B$ where $D_L(z) = H_0 d_L(z)$ is the "Hubble-constant-free" luminosity distance (throughout this paper we will follow the convention to use capital letters for Hubble-constant-free distances and small letters for distances measured in Mpc. Different papers use different conventions.). The measurement of μ_B is only a relative measurement and $\mathcal{M}_B$ allows for an additive uncertainty which can be left as a nuisance parameter. To simplify our notation, we absorb $5\log_{10}(H_0) - 25$ into our definition of the distance modulus, leading to:

$$\begin{aligned}\tilde{\mu}_B &= m_B - \mathcal{M}_B = \mu_B + 5\log_{10}(H_0) - 25\\ &= 5\log_{10}[D_L(z)]. \qquad (8)\end{aligned}$$

With this definition of the distance modulus we have calibrated the overall offset of the data to be zero. When fitting the data, we allow for a systematic calibration shift error, used to move the entire distance modulus data set up or down. To account for uncertainties in this calibration, we introduce a shift parameter Δ_μ with a broad uniform prior. The expected value for Δ_μ is zero.

B. BAO Measurements

Baryon acoustic oscillations provide another powerful measurement of the expansion history of the Universe. In a manner similar to supernovae they yield a geometric probe of dark energy. By carrying out measurements of the clustering along the transverse BAO scale one can obtain the angular diameter distance $d_A(z)$, defined as

$$d_A(z) = \frac{1}{1+z}\frac{c}{H_0}\int_0^z \frac{ds}{h(s)}, \qquad (9)$$

and by measuring the BAO scale along the line of sight, one obtains information on the Hubble parameter $H(z)$ itself (for details on future measurements, see, e.g. Ref. [6]). Both of these measurements will be scaled by the sound horizon at the epoch of baryon drag, $r_s(z_d)$, as given by:

$$r_s(z_d) = \frac{c}{\sqrt{3}}\int_{z_d}^\infty \frac{ds}{H(s)\sqrt{1+\frac{3\Omega_b}{4\Omega_\gamma(1+s)}}}, \qquad (10)$$

the final measurements being in terms of $d_A(z)/r_s$ and $H(z)r_s$. Current data provide information only on the angular diameter distance. The structure of Eq. (9) with respect to its w-dependence via two integrals is exactly the same as for $d_L(z)$ given in Eq. (1). This greatly simplifies the task of performing $w(z)$ reconstruction combining both probes.

C. CMB Measurements

For the CMB measurements we employ the so-called shift parameter $R(z_\star)$ first introduced by Bond et al. [21]:

$$R(z_\star) = \frac{\sqrt{\Omega_m H_0^2}}{c}(1+z_\star)d_A(z_\star) = \sqrt{\Omega_m}\int_0^{z_\star}\frac{ds}{h(s)}, \quad (11)$$

where $z_\star$ is the redshift of decoupling ($z_\star \sim 1090$) and the angular diameter distance d_A is given in Eq. (9). The shift parameter is related to the peak heights and the locations of the peaks in the temperature power spectrum of the CMB. As we will show in our analysis below, the shift parameter is very helpful in breaking the degeneracy between Ω_m and $w(z)$ when used in a combined analysis with supernova data. As an alternative to using the full CMB power spectra, the shift parameter provides a good way to summarize (see, e.g., Ref. [22]) CMB measurements, hence simplifying dark energy investigations.

One caveat of using R as pointed out in, e.g., Ref. [20] is the fact that R is a derived quantity from fitting to the CMB power spectrum and therefore assumes a certain cosmology. It is therefore important to state explicitly the assumption made under which the best-fit value for R was derived. Several groups including Refs. [22–24] have studied this point in more detail and found that the constraints on R are relatively stable under minor modifications of the dark energy parameters underlying the analysis, including dark energy clustering [24]. It was found that massive neutrinos had a larger effect on R (few percent level) [24]. In Ref. [22] an analysis of WMAP-3 data was carried out and it was found that for non-flat cosmologies, the value for R was similar for different dark energy models, including constant w and time-varying w parametrized via $w_0 + w_a(1-a)$. In addition, the best-fit values for R in the current WMAP-7 analysis are the same within error bars for different underlying cosmologies, including wCDM and open wCDM models.

In our analysis of currently available data it should be kept in mind that we use the best-fit value for R derived under the assumptions of a flat FRW universe with $w = -1$, an effective number of neutrinos of $N_{\rm eff} = 3.04$ and a primordial power spectrum close to a power law. As we show below, the inclusion of R in the analysis in addition to the supernova data does not alter the result for $w(z)$ itself, its main contribution is to help relax the assumption on Ω_m. For this reason, the fact that the value we use for R is derived for a specific model is of much less consequence. With future data from Planck the uncertainty on R will be as low as 0.2% at which point this issue has to be revisited in detail. In the case of our simulated data, the value of R is obtained for the correct underlying cosmology, in which case the above discussion does not apply.

Another issue arises with the CMB measurement point due to its origin at high redshift. The SNe and BAO data points occupy a redshift range between $z \in (0,2)$ making it easier to set up a coherent non-parametric reconstruction approach. The CMB data point on the other hand is a single point around $z \sim 1000$, so far away that it is bound to cause problems for any non-parametric method. Consequently, we have to make some assumptions about the behavior of $w(z)$ in the range $z \in (2,\infty)$ – the simplest choice is $w = const.$ Therefore, for the regime where we do not have SNe data, we assume $w = const.$ and find the best-fit value.

III. RECONSTRUCTION WITH GAUSSIAN PROCESS MODELING

A. Overview

Our nonparametric reconstruction method based on GP modeling and Markov chain Monte Carlo (MCMC), with application to supernova data is described in Refs. [18, 19]. We refer the reader to these papers for details on the implementation of the GP model. Here, we provide a general introduction and explanation of the idea behind the reconstruction process with GP models and then focus on how to extend the method to include multiple data sources.

Gaussian processes extend the multivariate Gaussian distribution to function spaces, with inference taking place in the space of functions. The defining property of a GP is that the vector that corresponds to the process at any finite collection of points follows a multivariate Gaussian distribution. Gaussian processes are elements of an infinite dimensional space, and can be used as the basis for a nonparametric reconstruction method. Gaussian processes are characterized by mean and covariance functions, defined by a small number of hyperparameters [25]. The covariance function controls aspects such as roughness of the candidate functions and the length scales on which they can change; aside from this, their shapes are arbitrary. The use of Bayesian estimation methods (including the MCMC algorithm) allows us to estimate the hyperparameters of the GP correlation function together with any other parameters, comprehensively propagating all estimation uncertainties [26].

Following the definition of a GP, we assume that, for any collection $z_1, ..., z_n$, $w(z_1), ..., w(z_n)$ follow a multivariate Gaussian distribution with a constant negative mean and exponential covariance function written as

$$K(z,z') = \kappa^2 \rho^{|z-z'|^\alpha}. \quad (12)$$

Here $\rho \in (0,1)$ is a free parameter that, together with κ and the parameters defining the likelihood, are fit from the data (ρ and κ are the hyperparameters of the GP model, for a more detailed discussion see Appendix A). The form of the assumed correlation function implies that, theoretically, there is non-zero correlation between any two points. The parameter ρ controls the exponential decay of the correlation as a function of distance in

redshift, but it does not provide a bound for the correlation between two points.

The value of $\alpha \in (0, 2]$ influences the smoothness of the GP realizations: for $\alpha = 2$, the realizations are smooth with infinitely many derivatives, while $\alpha = 1$ leads to rougher realizations suited to modeling continuous non-differentiable functions. Here we use $\alpha = 1$ to allow for maximum flexibility in reconstructing w. (For a comprehensive discussion of different choices for covariance functions and their properties, see Ref. [25].) We set up the following GP for w:

$$w(u) \sim \mathrm{GP}(\vartheta, K(u, u')). \tag{13}$$

The process is started using a mean value of $\vartheta = -1$; given current observational constraints on w this is a natural choice. Even though the mean is fixed, each GP realization actually has a different mean with a spread controlled by κ and the means are adjusted during the analysis to slightly different values suggested by preliminary runs (we use this strategy for some of the simulated data sets below). This adjustment is informed purely by the data and demonstrates the flexibility of the approach. In principle, the mean could also be left as a free parameter. After the adjustment we measure the posterior mean and ensure that it is close to the prior mean.

B. Combining Multiple Data Sources

In order to determine the optimal values for the GP modeling parameters and the cosmological parameters, we follow a Bayesian analysis approach [27]. We use MCMC algorithms to fit for the parameters [26], resulting in posterior estimates and probability intervals for Ω_m and Δ_μ, and the hyperparameters that specify the GP model, κ and ρ. We choose the following priors for the hyperparameters:

$$\pi(\kappa^2) \sim IG(6, 2), \tag{14}$$
$$\pi(\rho) \sim Beta(6, 1). \tag{15}$$

Here the notation "$\sim$" means "distributed according to", and IG is an inverse Gamma distribution prior, with the probability density function $f(x; \alpha, \beta) = \beta^\alpha x^{-\alpha-1}\Gamma(\alpha)^{-1}\exp(-\beta/x)$, with $x > 0$. The probability distribution of the $Beta$ prior is given by $f(x; \alpha, \beta) = \Gamma(\alpha+\beta)x^{\alpha-1}(1-x)^{\beta-1}/[\Gamma(\alpha)\Gamma(\beta)]$ (for examples of these distributions, see, e.g., Ref. [19]).

Turning to the cosmological parameters, we choose:

$$\pi(\Omega_m) \sim N(0.27, 0.04^2) \quad \text{SN data only}, \tag{16}$$
$$\pi(\Omega_m) \sim U(0, 1) \quad \text{combined analyses}, \tag{17}$$
$$\pi(\Delta_\mu) \sim U(-0.5, 0.5), \tag{18}$$
$$\pi(\sigma^2) \propto \sigma^{-2} \quad \text{SN data}, \tag{19}$$
$$\pi(\sigma_B^2) \propto \sigma_B^{-2} \quad \text{BAO data}, \tag{20}$$

where U is a uniform prior, with the probability density function $f(x; a, b) = 1/(b-a)$ for $x \in [a, b]$ and zero otherwise. N is a Gaussian (or Normal distributed) prior with the probability density function $f(x; \mu, \sigma^2) = \exp[-(x-\mu)^2/(2\sigma^2)]/\sqrt{2\pi\sigma^2}$. The squared notation for the second parameter in $N(\mu, \sigma^2)$ is used to indicate that σ is the standard deviation (to prevent possible confusion with the variance σ^2). (The parameters in the U and IG distributions do not have this same meaning of mean and standard deviation as in the Normal distribution.) σ^2 and σ_B^2 are the variable variance parameters associated with the SNe and BAO measurements respectively.

The prior for Ω_m for the analysis of supernova data alone is informed by the 7-year WMAP analysis [20] for a wCDM model combining CMB, BAO, and H_0 measurement. Once a second cosmological probe is included in the analysis, the assumption on this prior can be relaxed and we choose a uniform prior for the analysis of the combined data sets. As mentioned previously, we also allow for uncertainty in the overall calibration of the supernova data, Δ_μ, and choose a wide, uniform prior for Δ_μ.

Next we discuss the likelihoods for the different probes. We assume that the SNe, CMB, and BAO measurements are independent of each other which allows us to derive a likelihood for each probe separately. The likelihood for the supernova data is given by:

$$L^{\mathrm{SN}}(\sigma, \theta) \propto \left(\frac{1}{\tau_i \sigma}\right)^n \exp\left(-\frac{1}{2}\sum_{i=1}^{n}\left(\frac{\mu_i - \mu(z_i, \theta)}{\tau_i \sigma}\right)^2\right), \tag{21}$$

where θ encapsulates the cosmological parameters as well as the hyperparameters, i.e., $\{\Delta_\mu, \Omega_m, \kappa, \rho\}$ and σ^2 is the associated variance, expected to be close to unity. τ_i is the standard error measure associated with the data points, resulting from, e.g., the light curve fitting process. We assume no correlation between supernova distance errors and do not include any systematic errors. Both of these would obviously degrade the error bands in a full analysis; we do not include them here to keep the analysis simpler, though our framework in principle allows for them. We have an equivalent expression for the CMB data:

$$L^{\mathrm{CMB}}(\theta) \propto \frac{1}{\tau_{z^*}} \exp\left(-\frac{1}{2}\left(\frac{y^* - R(z^*, \theta)}{\tau_{z^*}}\right)^2\right). \tag{22}$$

Since we only have one data point, we cannot assign a variance parameter.

The likelihood for the BAO data is slightly more complicated. For future surveys, for each BAO point we will have two observed distance measures. These measurements (y_{1i}, y_{2i}) are correlated and we assume that they have a correlated and bivariate Normal distribution, given by:

$$\begin{bmatrix} y_{1i} \\ y_{2i} \end{bmatrix} \sim MVN\left[\begin{bmatrix} D_A(z_i)/r_s \\ H(z_i) * r_s \end{bmatrix}, \sigma_B^2 \mathbf{K}\right], \tag{23}$$

where

$$\mathbf{K} = \begin{bmatrix} \sigma_{y_{1i}}^2 & r_{12i}\sigma_{y_{1i}}\sigma_{y_{2i}} \\ r_{21i}\sigma_{y_{1i}}\sigma_{y_{2i}} & \sigma_{y_{2i}}^2 \end{bmatrix}, \tag{24}$$

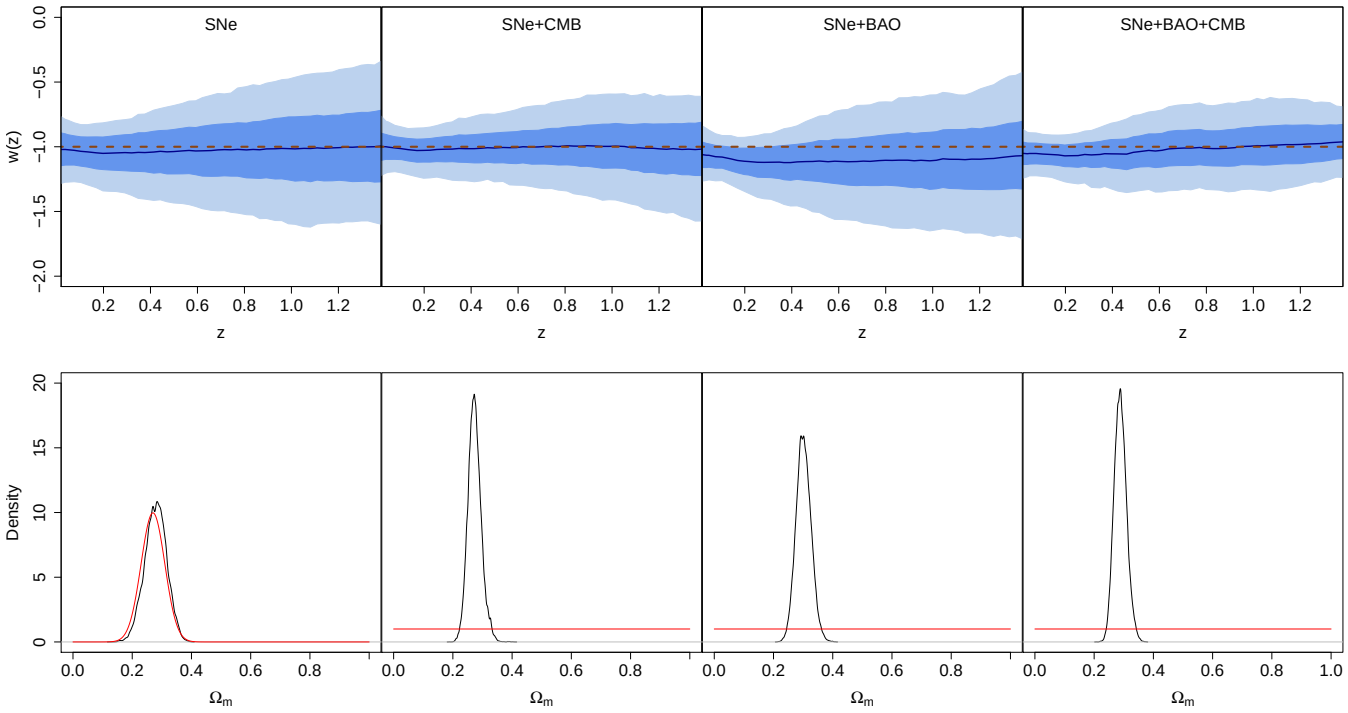

FIG. 1. Results for reconstructing $w(z)$ from currently available data. The top row shows reconstruction results for $w(z)$ (blue line; the red dashed line shows $w = -1$) for an exponential covariance function, i.e. $\alpha = 1$, including different cosmological probes, the second row shows the corresponding posterior for Ω_m (red lines: priors, black lines: posteriors). The first column shows the results from supernova data only, the second column includes CMB measurements, the third column uses supernova and BAO data, and the fourth column shows the results for a combined supernova-BAO-CMB analysis. The light blue contours show the 95% confidence level, the dark blue contours the 68% confidence level. As is to be expected, the error bars shrink somewhat if more data sources are included, though the effect is small due to the limited number of extra data points. As found previously by others (e.g., Ref. [13]), current data are consistent with a cosmological constant.

TABLE I. Union 2 Data set- 95% PIs, the last two columns are results from Ref. [13], Table 11 for comparison.

Data Type	Ω_m	Δ_μ	σ^2	ρ	κ^2	ϑ	Ω_m [13]	w [13]
SNe	$0.279^{+0.070}_{-0.074}$	$-0.003^{+0.028}_{-0.028}$	$0.985^{+0.124}_{-0.110}$	$0.870^{+0.127}_{-0.303}$	$0.353^{+0.393}_{-0.192}$	-1.00	$0.270^{+0.021}_{-0.021}$	-1 (fixed)
SNe+BAO	$0.302^{+0.051}_{-0.048}$	$-0.004^{+0.028}_{-0.027}$	$0.981^{+0.122}_{-0.109}$	$0.864^{+0.132}_{-0.322}$	$0.363^{+0.437}_{-0.202}$	-1.07	$0.309^{+0.032}_{-0.032}$	$-1.114^{+0.098}_{-0.112}$
SNe+CMB	$0.274^{+0.049}_{-0.041}$	$-0.002^{+0.028}_{-0.027}$	$0.982^{+0.123}_{-0.109}$	$0.865^{+0.132}_{-0.333}$	$0.358^{+0.447}_{-0.199}$	-1.00	$0.268^{+0.019}_{-0.017}$	$-0.997^{+0.050}_{-0.055}$
SNe+BAO+CMB	$0.289^{+0.044}_{-0.038}$	$-0.005^{+0.027}_{-0.027}$	$0.981^{+0.122}_{-0.109}$	$0.869^{+0.127}_{-0.302}$	$0.366^{+0.436}_{-0.201}$	-1.01	$0.277^{+0.014}_{-0.014}$	$-1.009^{+0.050}_{-0.054}$

and σ_B is the associated variance parameter. This leads to the following likelihood for the BAO data:

$$L^{\rm BAO}(\sigma_B,\theta) \propto \frac{1}{|\sigma_B^2\mathbf{K}|^{m/2}} \exp\left(-\frac{1}{2\sigma_B^2}\sum_{i=1}^{m}\left(\mathbf{D}^T\mathbf{K^{-1}}\mathbf{D}\right)\right), \tag{25}$$

with

$$\mathbf{D} = \begin{pmatrix} y_{1i} - D_a(z)/r_s \\ y_{2i} - H(z) * r_s \end{pmatrix}. \tag{26}$$

Current measurements yield data only for $T(z) = r_s(z_d)/d_V(z)$, where $d_V(z) = [(1+z)^2 d_A^2 cz/H(z)]^{1/3}$. The likelihood given in Eq. (25) therefore simplifies for current BAO data to

$$L^{\rm BAO}(\sigma_B,\theta) \propto \left(\frac{1}{\tau_i\sigma}\right)^m \exp\left(-\frac{1}{2}\sum_{i=1}^{m}\left(\frac{y_i^* - T(z_i)}{\tau_i\sigma_B}\right)^2\right), \tag{27}$$

with $m = 2$. We will use Eq. (25) for the simulated data and Eq. (2) for the real data.

We can find the combined likelihood simply by multiplying the individual likelihoods since we assume the different probes are uncorrelated:

$$L^{\rm total} = L^{\rm SNe} * L^{\rm CMB} * L^{\rm BAO}. \tag{28}$$

IV. RESULTS FOR CURRENT OBSERVATIONS

We begin our analysis by reconstructing $w(z)$ from currently available data. We use the supernova data set recently released by Amanullah et al. [13]. This so-called Union-2 compilation (extending the Union compilation from Ref. [28]) consists of 557 supernovae between redshift $z = 0.015$ and $z = 1.4$. The magnitude errors in the data set range between 0.08 and 1.02, with an average error of ~ 0.2.

In addition to the supernova data we include the most recent BAO measurements from the Two-degree-Field Galaxy Redshift Survey (2dFGRS) at $z = 0.2$ and the Sloan Digital Sky Survey (SDSS) [29] at $z = 0.35$ given by

$$r_s(z_d)/d_V(z = 0.2) = 0.1905 \pm 0.0061, \quad (29)$$

$$r_s(z_d)/d_V(z = 0.35) = 0.1097 \pm 0.0036. \quad (30)$$

For the CMB analysis, we use the most recent measurement of the shift parameter R from WMAP-7 [20], given by

$$R(z_\star) = 1.719 \pm 0.019. \quad (31)$$

In order to have a complete description of the problem we have to specify some additional cosmological parameters that are expected to have little or no effect on dark energy. These parameters – fixed at the best-fit WMAP-7 values from their ΛCDM analysis – are: $\Omega_\gamma = 4.897{\cdot}10^{-5}$, $z_d = 1020.3$, $z_\star = 1090.79$, and $\Omega_b/\Omega_\gamma = 914.54$.

We carry out four different analyses: supernova data by themselves with a Gaussian prior for Ω_m given in Eq. (16), and combined analyses for supernova data and CMB, supernova data and BAO, and for all three probes. For the combined data sets we can relax the prior assumptions on Ω_m and use a wide uniform prior, given in Eq. (17). The results are summarized in Table I and Figure 1.

All results are consistent with a cosmological constant, i.e. $w = -1$, as can be seen in the first row in Figure 1. The supernova data by themselves have only modest constraining power on Ω_m and therefore force us to choose a rather strong prior. The lower panels in Figure 1 show the prior (red line) and posterior (black line) for Ω_m demonstrating this point clearly. If we include either CMB or BAO or both, the constraints on Ω_m get much better. As can been seen in Table I, the error estimates for Ω_m shrink by almost a factor of two if all probes are combined. Overall, the supernova data by themselves lead to a slightly lower value of Ω_m, while the combination with CMB data leads to a higher value. The inclusion of the BAO points shifts up the value for Ω_m considerably, by more than 10% compared to the supernova–CMB analysis. Nevertheless, within the error bars, all values for Ω_m are consistent and agree well with the best-fit WMAP-7 values including different probes (e.g. for a ΛCDM model including CMB, BAO, and SNe data they find $\Omega_m = 0.278 \pm 0.015$). The value for the shift parameter Δ_μ is very close to zero in all cases.

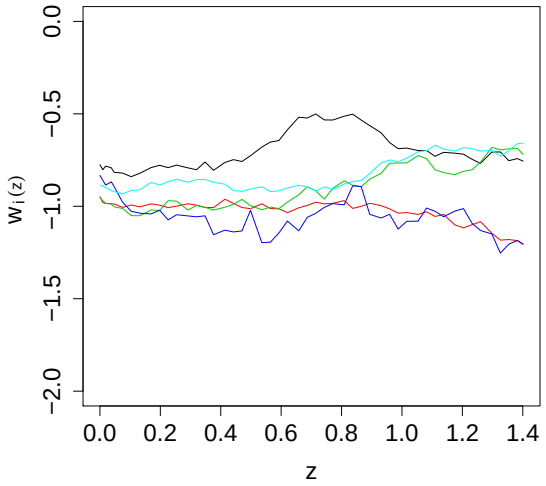

FIG. 2. A few random GP realizations for $w(z)$ for the SNe-only data (left upper panel in Figure 1).

A brief check against the results of Ref. [13] also shows very good agreement. For ease of comparison, we quote their results in the last two columns of Table I for the case of a flat Universe and $w = const.$ The trends in the best-fit value for Ω_m are exactly the same as we find, the value is lowest for the case of supernova+CMB data and highest for supernova+BAO data. They also find that for the supernova+BAO analysis, w is slightly below $w = -1$ while for all other cases it is very close to $w = -1$. Their analysis is also consistent with a cosmological constant. It is interesting to note that our error estimates for $w(z)$ are similar to the findings of Amanullah et al., even though their assumption of $w = const.$ is more restrictive. This shows that our method leads to tight error bounds without loss of flexibility in allowing for time variations in $w(z)$.

To underline this flexibility, we show a handful of realizations of the accepted GP trajectories in Figure 2. (Trajectories such as these make up the error bands for $w(z)$.) The trajectories show that the GP approach easily allows for substantial variation in the z-dependence of $w(z)$ with only modest smoothness restrictions. The trajectories allow for much more flexibility than the more traditional parametric forms, such as a w_0-w_a parametrization. As we show in the Appendix, the smoothness assumption can be relaxed if desired by choosing less informative priors for the hyperparameters ρ and κ^2. In this case, much "noisier" $w(z)$ trajectories can be incorporated, but their physical relevance is doubtful. We believe that the choice of hyperparameter priors made here is a sensible one, providing a good balance between allowed variability and noise within individual trajectories.

The realizations also show that interpretation of the correlation length ($\lambda = -1/\ln\rho$) requires some care. The

correlation length refers to a statistical average across all trajectories and does not directly address the perceived variability of individual realizations. In particular, the correlation length is not determined by the range over which the data has been gathered but by the behavior of the data and by the size of the observational errors. The variability of individual realizations is also determined by the normalization amplitude as set by κ^2 (see Appendix A for further discussion). Thus, the values for ρ close to one that we find do not imply that our reconstruction results cannot pick up variations in $w(z)$ spanning redshift ranges on scales smaller than the range investigated in the data.

V. RESULTS FOR SIMULATED DATA

In this section we investigate how well our method works for reconstructing $w(z)$ with future high-quality data. Current limitations – uncertainties in the data and limited statistics – prevent us from extracting possible time variations in $w(z)$ reliably. The error bands are relatively large and results are in complete agreement with a cosmological constant. Future measurements will hopefully change this: if there is a small time variation in $w(z)$ we should be able to detect it. In a previous paper [18], we generated a supernova data set, assuming high-quality measurements from a WFIRST-like mission. We showed that a set of $\sim$ 2300 supernovae out to a redshift of $z = 1.7$ and perfect knowledge of Ω_m allows us to confidently extract time variations in the dark energy equation of state. We also showed that larger uncertainties in Ω_m degraded this result due to well-known degeneracies between w and Ω_m. These degeneracies can be broken by including different data sources. We show in the following that a combination of accurate supernova data with results from a BAO survey such as BigBOSS will provide sufficient information to enable a reliable and interesting reconstruction of $w(z)$. The combination of these different data sources eliminates the degeneracy problem and provides reliable constraints on the time variation of $w(z)$ without requiring "perfect" knowledge of Ω_m.

A. The Simulated Data

We generate simulated data for all three probes (supernovae, BAO, CMB) and three different cosmological models. The models used are the same as in our previous work (see Ref. [18] for more details). Model 1 has a constant dark energy equation of state $w = -1$, Model 2 is based on a quintessence model with a minimally coupled scalar field and a dark energy equation of state $w(z) = (\dot{\phi}/2 - V_0\phi^2)/(\dot{\phi}^2/2 + V_0\phi^2)$, and for Model 3 we choose a slightly more extreme quintessence model with $w(z) = -1.0006 + 308472/(\exp[20/(1+z) + 617439])$. The resulting equations of state are shown in Figure 3. For each model we choose $\Omega_m = 0.27$ and fix $H_0 = 70.4$ km/s/Mpc, $\omega_b = 0.0226$, $\omega_\gamma = 2.469 \cdot 10^{-5}$, $z_\star = 1090.89$, and $z_d = 1020.5$. While Model 3 is already ruled out observationally, it provides a good example for a rather sharp transition in $w(z)$. For each model we create two data sets: (i) We assume the best-possible scenario, a space mission to obtain supernova measurements out to redshift $z = 1.7$ and in addition a BigBOSS-like BAO survey, and CMB data; (ii) good ground-based supernova measurements in combination with BigBOSS and CMB measurements. In the following we provide some details on the assumptions for the different data sets.

1. *Supernova Measurements*

As mentioned above we investigate two different sets of simulated supernova measurements. The first one is the same as used in Ref. [18]. It contains 2298 data points distributed over a redshift range of $0 < z < 1.7$ with larger concentration of supernovae in the midrange redshift bins ($0.4 < z < 1.1$) and at low redshift ($z < 0.1$). The exact distribution is shown in Ref. [18] in Figure 1. For the distance modulus we assume an error of $\tau_i = 0.13$. The measurements are presented in the following form:

$$\tilde{\mu}_i = \alpha_i + \epsilon_i. \tag{32}$$

In this notation, the observations $\tilde{\mu}_i$ follow a normal distribution with mean $\alpha(z_i)$, the standard deviation being set by the distribution of the error, ϵ_i, representing a mean-zero normal distribution with standard deviation, $\tau_i\sigma$. Here, τ_i is the observed error and σ accounts for a possible rescaling. In addition, we assume that the errors are independent.

For the second set of simulated supernova data we consider the same number of data points as currently available from ground-based surveys, augmented with some

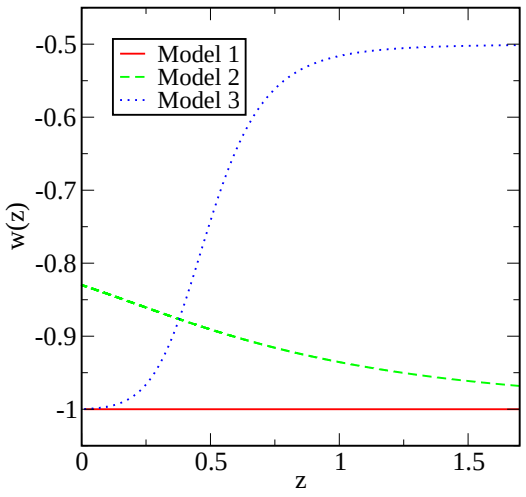

FIG. 3. Dark energy equation of state $w(z)$ for our three simulated models.

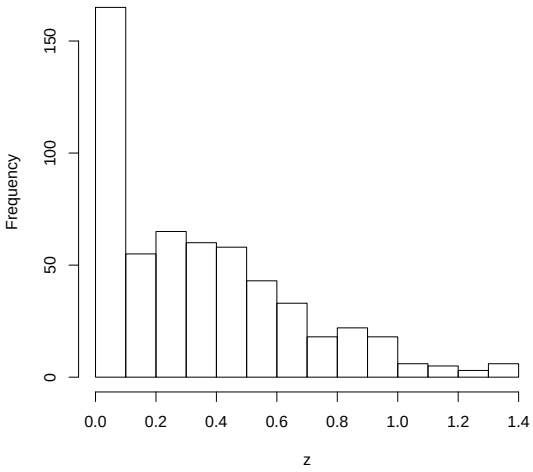

FIG. 4. Redshift distribution of the small supernova data set. The simulated data has exactly the same distribution as the real data.

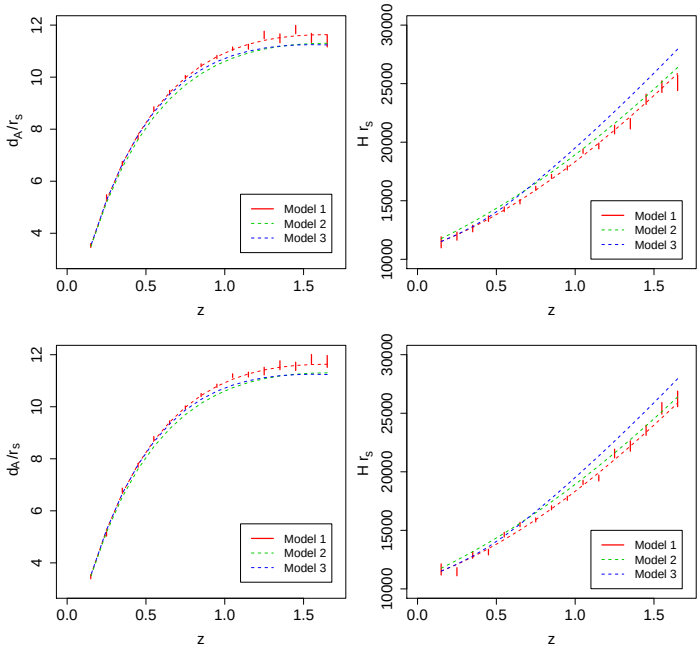

FIG. 5. Two realizations of 20 simulated BAO points for a BigBOSS-like survey. Left column: angular distance diameter, right column: Hubble parameter, both appropriately scaled by the sound horizon as relevant to BAO measurements. Model 1 ($w = const.$) is shown with error bars with one standard deviation. For Model 2 (green dashed) and Model 3 (blue dotted) we show the exact predictions.

higher redshift observations such as those that have been obtained with the Hubble Space Telescope (557 measurements total). The redshift distribution is shown in Figure 4. The distribution extends to $z = 1.4$ with a maximum at low redshift and around $z = 0.3$. Only a handful of supernovae are available at higher redshifts. Since we assume that the measurements are of somewhat lower quality, we increase the errors on the distance modulus to $\tau_i = 0.15$.

2. *CMB Measurements*

For the CMB points we use the following realizations (the exact values for R for each model are given in parentheses):

$$\text{Model 1}: R(z_\star) = 1.736 \pm 0.019 (R^{\rm ex} = 1.723), \quad (33)$$
$$\text{Model 2}: R(z_\star) = 1.716 \pm 0.019 (R^{\rm ex} = 1.702), \quad (34)$$
$$\text{Model 3}: R(z_\star) = 1.683 \pm 0.019 (R^{\rm ex} = 1.670). \quad (35)$$

3. *BAO Measurements*

Future BAO surveys such as BigBOSS will obtain measurements of the angular diameter distance, $d_A(z)$, as well as the Hubble parameter $H(z)$, in terms of the sound horizon at the epoch of baryon drag, $r_s(z_d)$. For our simulated BAO data sets, we follow the specifications for a BigBOSS survey as outlined in http://bigboss.lbl.gov/docs/BigBOSS_NOAO_public.pdf. We assume a survey area of 24000 deg^2 (covering northern and southern skies) and adopt the galaxy density distribution estimated in the BigBOSS proposal (Table 2.3 in the aforementioned document). In this proposal, measurements from luminous red galaxies and emission-line galaxies are combined. The resulting distribution accounts for several sources of inefficiency (discussed in the BigBOSS proposal) leading to a degradation of the galaxy number density at high redshift. Often a constant galaxy density over the whole redshift range is assumed. We studied this case as well and found that the eventual results in both cases are very similar. In order to derive estimates for the errors of the simulated measurements, we use a publicly available code from Ref. [30]. The formula used to obtain BAO errors in this code is a 2D approximation of the full Fisher matrix formalism. In Ref. [30], the results for the full Fisher matrix calculation and this method are shown to match well. Although these results are for ΛCDM, they should hold reasonably well for other cosmologies.

The input parameters for the code are: σ_8 at the present epoch, $\Sigma_\perp = \Sigma_0 G$ = transverse *rms* Lagrangian displacement, with G = growth factor normalized such that $G = (1+z)^{-1}$ at high redshift, $\Sigma_0 = 12.4h^{-1}$ Mpc for a cosmology with $\sigma_8 = 0.9$ at present and scaling linearly with σ_8; $\Sigma_\parallel = \Sigma_0 G(1+f)$ = line of sight *rms* Lagrangian displacement, with $f = d(\ln G)/d(\ln a), G, \Sigma_0$ as before; and the number density $= 3 \times 10^{-4} h^3/\text{Mpc}^3$ (Cf. Ref. [6]). G, f, σ_8 are input correctly for each model.

The biggest possible source of error are the formulae used for $\Sigma_\perp, \Sigma_\parallel$; these were shown to be reasonable fits to the true values in Ref. [31]. The value of Σ_0 given is also for the cosmology used in Ref. [31]. For a different cosmology, Σ_0 would obviously be different, and the simplest way to deal with this, as suggested in the paper, is to scale it linearly with σ_8. This may not be completely accurate as we use very different cosmological models but should yield a reliable estimate.

Figure 5 shows two realizations for a ΛCDM model (Model 1) for the angular distance diameter $D_A(z)/r_s$ in the left column and for the Hubble parameter $H(z)r_s$ in the right column. In addition, we show the exact predictions for Model 2 and 3. We use two realizations for the BAO data to demonstrate the dependence of the reconstruction as a function of realization. Because observations represent only one realization, this imposes an an irreducible limitation on the reconstruction program, whether non-parametric or not. We will return to this issue in future work.

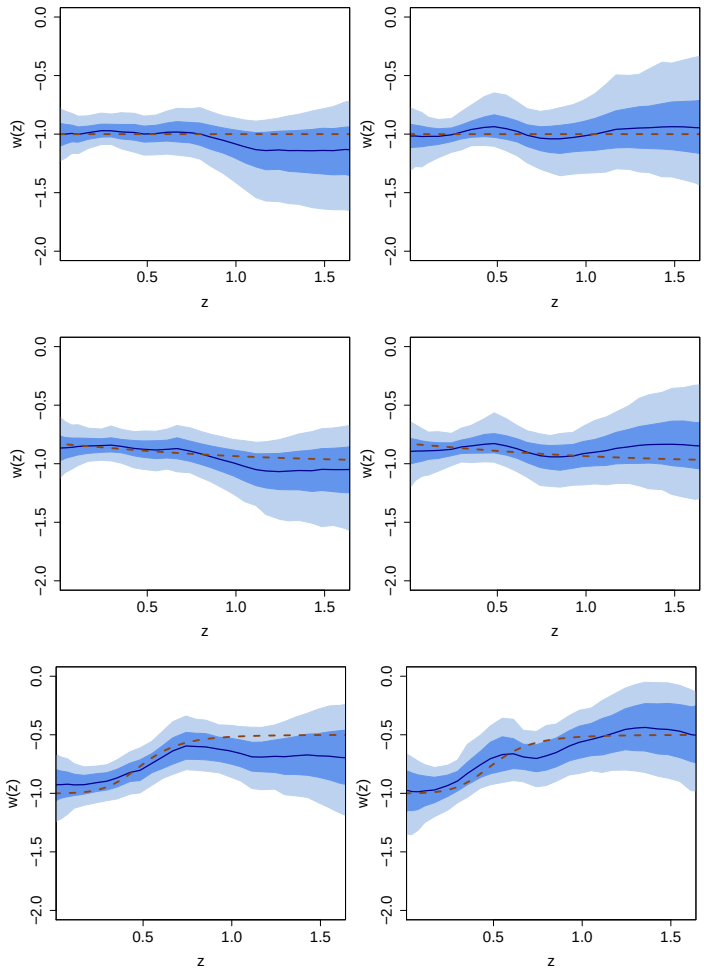

FIG. 6. Left column: reconstruction result for $w(z)$ for realization I of the BAO data later used in combination with the small supernova sample. Right column: results for realization II later used in combination with the large supernova sample. Top to bottom: results for Models 1 - 3. The dashed line shows the underlying theoretical model, the dark blue region shows the 68% confidence level, the light blue region the 95% confidence level, the dark blue line shows the mean reconstructed history. The error bands represent the single realization reconstruction error. In all cases, the reconstruction results capture the "truth" within the error bands reliably.

B. Results

1. *Prelude*

Before we present our results for the combined analysis of different cosmological probes we show the constraints we obtain from the simulated BAO data alone on $w(z)$. The results are already remarkably good. We choose a flat prior for Ω_m for this analysis.

Figure 6 shows the results for both realizations presented in Figure 5, Table II provides the best fit values for Ω_m all three models for the left column (Realization I) and Table III for the right column (Realization II). For Model 1 (first row) the predictions are slightly low for the first realization but overall the results are consistent with the input model., $w = -1$. We verified that this result does not change considerably if we tighten the prior on Ω_m. Similar trends can be seen for Model 2 and 3. We will come back to these trends later in the discussion on the results for combined data sets. The value for Ω_m for realization I (Table II) is slightly high in all cases – adding CMB measurements decreases the error on Ω_m but in fact shifts the best fit values even higher. The second realization leads to values for Ω_m very close to the input value for BAO measurements only, the CMB point again shifts it up slightly. The reconstruction from the BAO data alone works remarkably well – in all cases the underlying model is captured within the error bars reliably.

2. *Combining Different Data Sets*

Next we present the results for Model 1 - 3 for several different combinations of data as discussed above:

Ground-based supernova mission (Figs. 7-9, upper rows; Table II):

- 557 supernovae out to $z = 1.4$, $\tau_i = 0.15$
- supernovae + CMB measurement
- supernovae + 20 BAO points (realization I)
- supernova + BAO + CMB measurements

Space-based supernova mission (Figs. 7-9, lower rows; Table III):

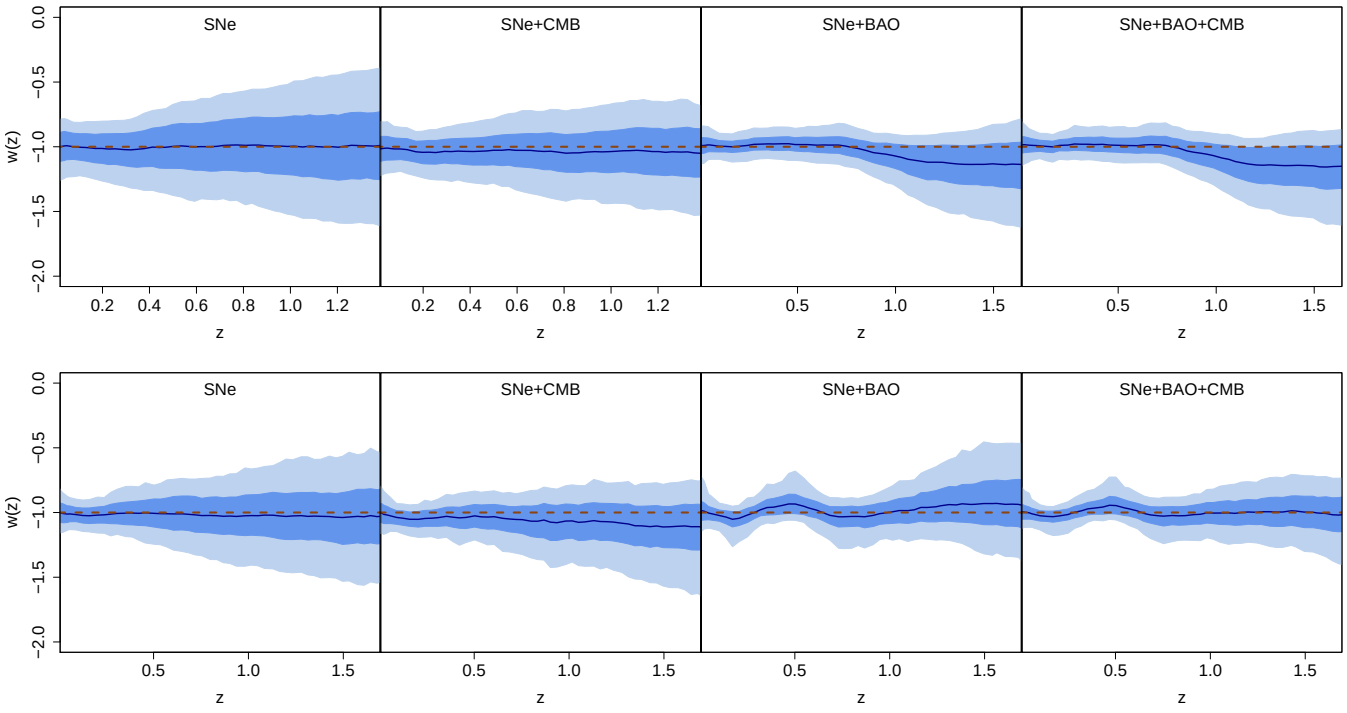

FIG. 7. Reconstruction results for the model with $w = -1$. From left to right different probes are considered, SNe, SNe+CMB, SNe+BAO, and a combination of all three measurements. The red dashed line shows the truth, the blue solid line the mean result for the reconstruction. The blue shaded region shows the 68% confidence level, the light blue shaded region the 95% confidence level. The upper row shows the results for the small supernova data set (557 supernovae with $\tau_i = 0.15$ out to $z = 1.4$) while the lower row shows potential space-based supernova measurements (2298 supernovae with $\tau_i = 0.13$ out to $z = 1.7$). The CMB data point is the same in all cases where it is included, the BAO data are of same quality but two different realizations out to $z = 2$. Note that the redshift range varies in the different panels depending on which probes are included.

- 2298 supernovae out to $z = 1.7$, $\tau_i = 0.13$
- supernovae + CMB measurement
- supernovae + 20 BAO points (realization II)
- supernova + BAO + CMB measurements

As for the real data, we choose a stronger prior for Ω_m in the case of analyzing supernova data only while we use a flat prior for any combination of data. Figure 7 shows the results for Model 1. The reconstruction from supernova data only works very well – the additional data points (comparing the upper and lower panel) help reduce the error bands (note that the redshift range in the lower row showing the results for 2298 supernovae extends out further) and also lead to a better estimate for Ω_m with tighter error bounds, given in Tables II, III. The addition of the CMB point (second column in Figure 7) allows us to choose a much less strict prior on Ω_m, i.e. a flat prior. Overall, the reconstruction works well with the combination of supernova and CMB measurements, the error bands on $w(z)$ shrinking considerably. The estimate for Ω_m is slightly too high leading to a small overall underestimation of $w(z)$ [we remind the reader of the degeneracy of Ω_m and $w(z)$].

In the third column we show the supernova+BAO analysis. In this case, both results extend to $z = 1.7$ due to the presence of BAO data at those redshifts. In the upper row, where the supernova data only covers a redshift range out to $z = 1.4$, the overall result is similar to the result from the BAO data only (Figure 6) though the error bands shrink considerably. Combining all three data sets leads to even narrower error bands (fourth column). In the lower row the small downward trend from the CMB point is compensated by the small upward trend from the BAO measurements at high redshifts, leading to an almost perfect reconstruction result. In the upper row, both CMB and BAO realizations have a small downward trend in $w(z)$ which is seen in the final result. Overall, the "truth" is captured well in all cases and lies well within the error bounds. We would like to emphasize that the dark blue line in the figures only represents the mean of the reconstruction result; much more significant are the error bands themselves – these must capture the true underlying model to establish a valid approach.

The results for Model 2 and 3 are similar, shown in Figures 8 and 9. Model 2 exhibits a small time variation which could be extracted from future data. The powerful

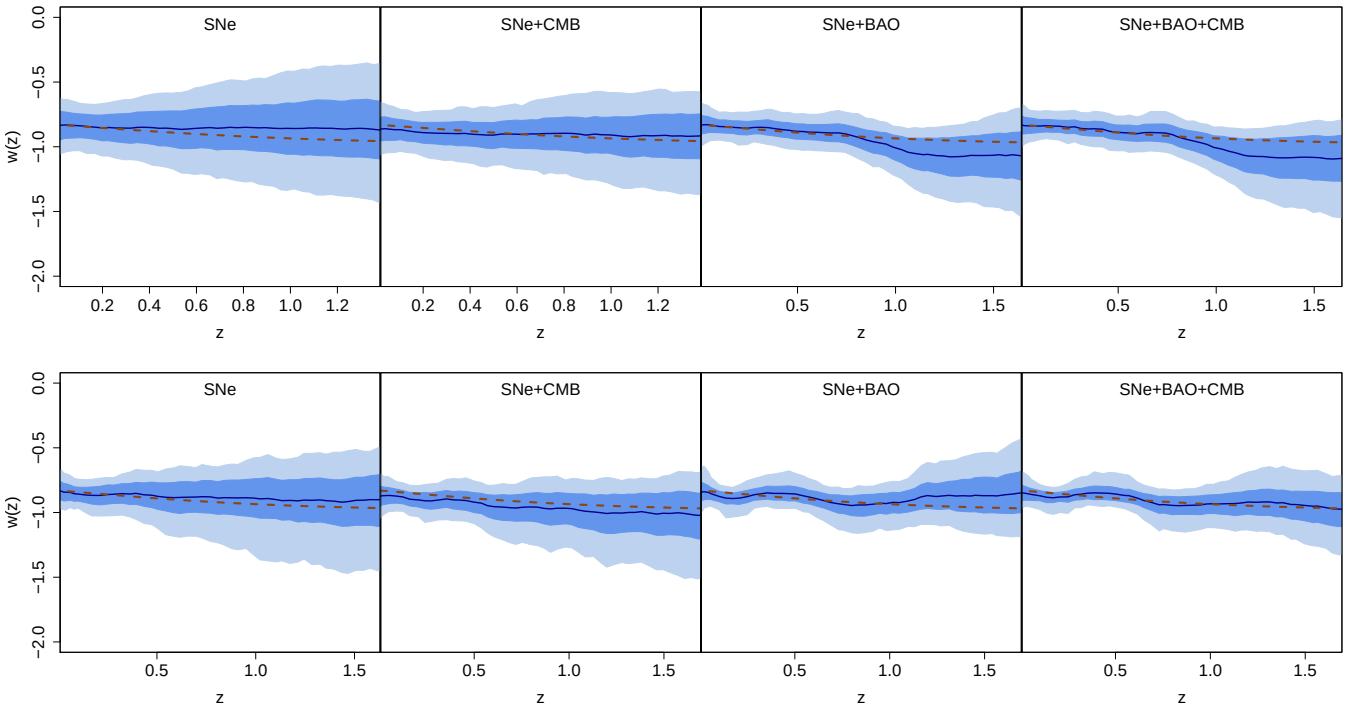

FIG. 8. Same as in Figure 7 but for Model 2, the quintessence model.

TABLE II. Posterior 95% PIs, 557 SNe points

Data Type	Data	Ω_m	Δ_μ	σ^2	σ_B^2	ρ	κ^2	ϑ
SNe	μ_1	$0.282^{+0.064}_{-0.069}$	$0.003^{+0.026}_{-0.027}$	$1.05^{+0.13}_{-0.12}$	n/a	$0.87^{+0.12}_{-0.30}$	$0.35^{+0.41}_{-0.19}$	-1.00
	μ_2	$0.277^{+0.070}_{-0.075}$	$0.002^{+0.026}_{-0.026}$	$1.05^{+0.13}_{-0.12}$	n/a	$0.88^{+0.12}_{-0.30}$	$0.35^{+0.40}_{-0.19}$	-0.87
	μ_3	$0.291^{+0.071}_{-0.082}$	$0.007^{+0.027}_{-0.027}$	$1.05^{+0.13}_{-0.12}$	n/a	$0.85^{+0.14}_{-0.30}$	$0.37^{+0.44}_{-0.21}$	-1.00
SNe+CMB	μ_1	$0.293^{+0.043}_{-0.038}$	$0.004^{+0.026}_{-0.026}$	$1.05^{+0.13}_{-0.12}$	n/a	$0.87^{+0.13}_{-0.30}$	$0.36^{+0.41}_{-0.20}$	-1.07
	μ_2	$0.297^{+0.046}_{-0.042}$	$0.002^{+0.026}_{-0.025}$	$1.05^{+0.13}_{-0.12}$	n/a	$0.87^{+0.12}_{-0.31}$	$0.36^{+0.45}_{-0.20}$	-0.94
	μ_3	$0.277^{+0.065}_{-0.050}$	$0.009^{+0.026}_{-0.026}$	$1.05^{+0.13}_{-0.12}$	n/a	$0.85^{+0.14}_{-0.31}$	$0.37^{+0.46}_{-0.21}$	-0.78
SNe+BAO	μ_1	$0.280^{+0.016}_{-0.015}$	$0.004^{+0.023}_{-0.022}$	$1.05^{+0.13}_{-0.12}$	$0.89^{+0.60}_{-0.37}$	$0.90^{+0.10}_{-0.26}$	$0.34^{+0.40}_{-0.18}$	-1.04
	μ_2	$0.280^{+0.017}_{-0.016}$	$0.002^{+0.024}_{-0.023}$	$1.05^{+0.13}_{-0.12}$	$0.88^{+0.60}_{-0.36}$	$0.88^{+0.11}_{-0.29}$	$0.34^{+0.40}_{-0.19}$	-0.94
	μ_3	$0.283^{+0.018}_{-0.019}$	$0.008^{+0.026}_{-0.026}$	$1.05^{+0.13}_{-0.12}$	$0.88^{+0.61}_{-0.37}$	$0.81^{+0.14}_{-0.26}$	$0.39^{+0.48}_{-0.22}$	-0.73
SNe+BAO+CMB	μ_1	$0.280^{+0.015}_{-0.015}$	$0.004^{+0.023}_{-0.023}$	$1.05^{+0.13}_{-0.12}$	$0.89^{+0.60}_{-0.36}$	$0.90^{+0.10}_{-0.26}$	$0.34^{+0.39}_{-0.18}$	-1.05
	μ_2	$0.280^{+0.016}_{-0.015}$	$0.002^{+0.024}_{-0.023}$	$1.05^{+0.13}_{-0.12}$	$0.88^{+0.60}_{-0.36}$	$0.88^{+0.11}_{-0.26}$	$0.35^{+0.40}_{-0.19}$	-0.95
	μ_3	$0.284^{+0.017}_{-0.017}$	$0.008^{+0.026}_{-0.025}$	$1.05^{+0.13}_{-0.12}$	$0.87^{+0.60}_{-0.36}$	$0.80^{+0.15}_{-0.26}$	$0.37^{+0.42}_{-0.20}$	-0.73
BAO	μ_1	$0.280^{+0.030}_{-0.028}$	n/a	n/a	$0.90^{+0.61}_{-0.37}$	$0.88^{+0.12}_{-0.30}$	$0.36^{+0.41}_{-0.19}$	-1.05
	μ_2	$0.276^{+0.035}_{-0.032}$	n/a	n/a	$0.89^{+0.62}_{-0.37}$	$0.86^{+0.13}_{-0.31}$	$0.34^{+0.38}_{-0.18}$	-0.92
	μ_3	$0.297^{+0.037}_{-0.044}$	n/a	n/a	$0.92^{+0.66}_{-0.39}$	$0.82^{+0.16}_{-0.28}$	$0.37^{+0.42}_{-0.20}$	-0.75
BAO+CMB	μ_1	$0.281^{+0.025}_{-0.024}$	n/a	n/a	$0.89^{+0.61}_{-0.37}$	$0.88^{+0.11}_{-0.28}$	$0.35^{+0.39}_{-0.19}$	-1.07
	μ_2	$0.279^{+0.029}_{-0.025}$	n/a	n/a	$0.89^{+0.61}_{-0.37}$	$0.88^{+0.12}_{-0.29}$	$0.35^{+0.41}_{-0.19}$	-0.95
	μ_3	$0.296^{+0.035}_{-0.035}$	n/a	n/a	$0.92^{+0.66}_{-0.39}$	$0.81^{+0.16}_{-0.31}$	$0.37^{+0.41}_{-0.20}$	-0.74

combination of all three probes can be gauged by the relatively small error bands shown in the fourth column in Figure 8. At low to intermediate redshifts (out to $z \sim 0.6$) a cosmological constant is clearly disfavored. The supernova data alone would not have had enough information to disfavor $w = -1$ at any redshift, as the error bands in this case clearly include a cosmological constant. The inclusion of high redshift supernova data improves the results somewhat, the overall reconstruction shown in the lower left corner of Figure 8 is excellent with narrow error bands. In this case, the constraints for Ω_m are also very close to the input value for the theoretical model with tight error bands.

Model 3 has a rather strong variation in $w(z)$. While this model is observationally ruled out already, it provides a good testbed for our new approach to demon-

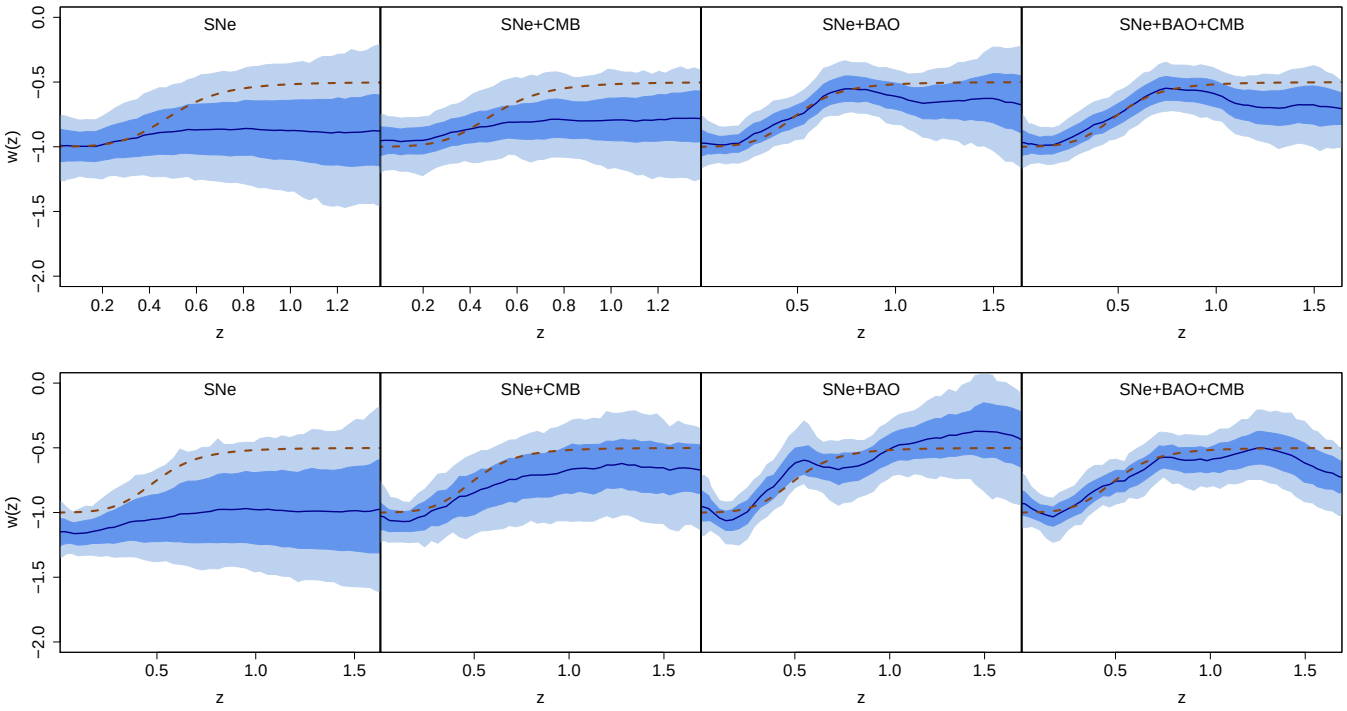

FIG. 9. Same as in Figure 7 but for Model 3.

TABLE III. Posterior 95% PIs, 2298 supernova

Data Type	Data	Ω_m	Δ_μ	σ^2	σ_B^2	ρ	κ^2	ϑ
SNe	μ_1	$0.270^{+0.032}_{-0.043}$	$-0.003^{+0.019}_{-0.018}$	$0.97^{+0.06}_{-0.05}$	n/a	$0.90^{+0.10}_{-0.27}$	$0.34^{+0.37}_{-0.18}$	-1.00
	μ_2	$0.263^{+0.046}_{-0.051}$	$-0.004^{+0.018}_{-0.018}$	$0.97^{+0.06}_{-0.06}$	n/a	$0.90^{+0.10}_{-0.27}$	$0.34^{+0.40}_{-0.18}$	-0.87
	μ_3	$0.327^{+0.040}_{-0.070}$	$-0.007^{+0.019}_{-0.019}$	$0.97^{+0.06}_{-0.06}$	n/a	$0.85^{+0.14}_{-0.32}$	$0.35^{+0.40}_{-0.19}$	-0.92
SNe+CMB	μ_1	$0.278^{+0.024}_{-0.024}$	$-0.003^{+0.020}_{-0.019}$	$0.97^{+0.06}_{-0.06}$	n/a	$0.89^{+0.11}_{-0.32}$	$0.34^{+0.39}_{-0.18}$	-1.04
	μ_2	$0.279^{+0.027}_{-0.026}$	$-0.006^{+0.019}_{-0.018}$	$0.97^{+0.06}_{-0.06}$	n/a	$0.90^{+0.10}_{-0.29}$	$0.34^{+0.38}_{-0.19}$	-0.90
	μ_3	$0.292^{+0.050}_{-0.043}$	$-0.002^{+0.021}_{-0.020}$	$0.97^{+0.06}_{-0.06}$	n/a	$0.81^{+0.16}_{-0.29}$	$0.40^{+0.48}_{-0.24}$	-0.82
SNe+BAO	μ_1	$0.269^{+0.011}_{-0.011}$	$-0.002^{+0.021}_{-0.019}$	$0.97^{+0.06}_{-0.06}$	$1.29^{+0.87}_{-0.54}$	$0.88^{+0.12}_{-0.36}$	$0.35^{+0.45}_{-0.20}$	-0.97
	μ_2	$0.269^{+0.011}_{-0.010}$	$-0.005^{+0.020}_{-0.018}$	$0.97^{+0.06}_{-0.06}$	$1.30^{+0.87}_{-0.54}$	$0.89^{+0.10}_{-0.28}$	$0.35^{+0.40}_{-0.19}$	-0.88
	μ_3	$0.268^{+0.013}_{-0.015}$	$-0.002^{+0.021}_{-0.022}$	$0.97^{+0.06}_{-0.06}$	$1.22^{+0.85}_{-0.52}$	$0.75^{+0.21}_{-0.32}$	$0.40^{+0.47}_{-0.22}$	-0.63
SNe+BAO+CMB	μ_1	$0.269^{+0.010}_{-0.010}$	$-0.001^{+0.018}_{-0.017}$	$0.97^{+0.06}_{-0.06}$	$1.31^{+0.88}_{-0.54}$	$0.90^{+0.10}_{-0.30}$	$0.35^{+0.42}_{-0.19}$	-1.00
	μ_2	$0.270^{+0.010}_{-0.010}$	$-0.004^{+0.018}_{-0.017}$	$0.97^{+0.06}_{-0.06}$	$1.31^{+0.88}_{-0.54}$	$0.91^{+0.09}_{-0.29}$	$0.34^{+0.40}_{-0.19}$	-0.90
	μ_3	$0.269^{+0.011}_{-0.011}$	$0.002^{+0.020}_{-0.021}$	$0.97^{+0.06}_{-0.06}$	$0.66^{+0.46}_{-0.28}$	$0.76^{+0.18}_{-0.31}$	$0.39^{+0.48}_{-0.21}$	-0.71
BAO	μ_1	$0.270^{+0.036}_{-0.049}$	n/a	n/a	$1.33^{+0.92}_{-0.56}$	$0.86^{+0.14}_{-0.31}$	$0.35^{+0.41}_{-0.20}$	-1.00
	μ_2	$0.264^{+0.037}_{-0.041}$	n/a	n/a	$1.33^{+0.92}_{-0.56}$	$0.87^{+0.13}_{-0.31}$	$0.35^{+0.40}_{-0.19}$	-0.88
	μ_3	$0.278^{+0.052}_{-0.059}$	n/a	n/a	$1.35^{+1.03}_{-0.60}$	$0.77^{+0.20}_{-0.30}$	$0.37^{+0.45}_{-0.20}$	-0.68
BAO+CMB	μ_1	$0.279^{+0.031}_{-0.025}$	n/a	n/a	$1.35^{+0.92}_{-0.56}$	$0.88^{+0.11}_{-0.31}$	$0.35^{+0.41}_{-0.19}$	-1.03
	μ_2	$0.275^{+0.032}_{-0.027}$	n/a	n/a	$1.35^{+0.93}_{-0.56}$	$0.88^{+0.11}_{-0.32}$	$0.36^{+0.43}_{-0.20}$	-0.92
	μ_3	$0.285^{+0.039}_{-0.044}$	n/a	n/a	$1.38^{+1.01}_{-0.62}$	$0.78^{+0.20}_{-0.32}$	$0.40^{+0.47}_{-0.22}$	-0.70

strate that more complicated dark energy equations of state can be reconstructed. As discussed in detail in Ref. [18] the degeneracy between Ω_m and $w(z)$ makes the reconstruction task rather difficult – the left panels in Figure 9 show the constructed $w(z)$ from supernova data only with a Gaussian prior on Ω_m. The error bars are rather wide and include a cosmological constant comfortably. The addition of the CMB point already improves the result considerably, in this case we choose a flat prior on Ω_m. The best-fit value for Ω_m is very close to the input value of 0.27 compared to the case where we analyze supernova data only. The inclusion of the BAO data (third and fourth column) in both cases (557 and 2298 supernova data points) improves the results even more. The time dependence is well captured and the estimate for Ω_m is also very good.

Some final remarks on the content of Tables II and III: in addition to the results discussed above, we provide some information on the results for the combination of BAO and CMB measurements. Overall, the extra information from the CMB measurement does not help very much to improve the results, contrary to what we find when we add this information to the supernova data. In addition to the constraints on the cosmological parameters and error behavior of the data (given by σ for the supernova data and σ_B for the BAO data) we list the final hyperparameters for the GP model in the last three columns. Perhaps the most interesting parameter here is the adjusted mean value for $w(z)$ given by ϑ in the last column. As described in Ref. [18] in detail, we start the GP model with some value for ϑ (in the case of Model 1, $\vartheta = -1$ is the natural choice for example) and run the reconstruction program for some time. The results then have information about an improved value for the mean of the GP model and the analysis framework can be adjusted accordingly. As can be seen in the Tables, the final values for ϑ are close to the mean value of the underlying truth. Because the adjustment scheme works extremely well, we started basically all reconstruction evaluations at $\vartheta = -1$, the GP model automatically suggesting better mean values if the choice was non-optimal. Overall, the reconstruction of $w(z)$ works very well when multiple sources are included.

VI. CONCLUSION

In this paper we have introduced a new non-parametric reconstruction scheme for the dark energy equation of state $w(z)$ combining multiple cosmological probes. The reconstruction scheme is based on a GP modeling approach and provides very good constraints on $w(z)$ with reliable error bars. The basic method was introduced in Ref. [18] for supernova data only. Here we extend the methodology to include BAO and CMB measurements. We have carried out an analysis of currently available data and found excellent agreement with a cosmological constant consistent with a large number of recent publications, including Refs. [12, 13, 20, 29]. We have also demonstrated our method on simulated data for different cosmological models. In all cases, the GP model approach performed very well.

An important aspect of our new approach (as stressed in Refs. [18, 19]) is the simultaneous constraint of the cosmological parameters as well as the hyperparameters of the GP model from the data. In comparison to parametric approaches, our new method is more flexible and can therefore capture even subtle time variations in $w(z)$ if the data quality is good enough. It produces narrow error bands over the full redshift ranges considered. For a more detailed comparison with parameterized methods, see Ref. [18].

The combination of different data probes mitigates the problem of degeneracies between $w(z)$ and Ω_m as is to be expected. An encouraging observation is that even the BAO data alone (of high quality from a BigBOSS-like survey) can deliver good constraints on the time dependence of the dark energy equation of state, clearly competitive with space based supernova observations.

Our new non-parametric reconstruction approach lends itself to analysis of the promise of future dark energy probes in a reliable way. For example, possible tension in the data due to, e.g., insufficient understanding of systematic errors would lead to an increase in the error bands when combining different probes (a different attempt to solve this problem with parametric methods is discussed in e.g. Ref. [32]). The GP based approach can therefore help to optimize future dark energy missions.

Appendix A: The GP Hyperparameters

The main feature that distinguishes the GP model approach from most other reconstruction schemes is the introduction of the so-called hyperparameters. The values for the hyperparameters are informed by the data sets themselves and determine the final outcome. Obviously, some assumptions have to be made and priors chosen for the hyperparameters. Fully non-informative priors in our case may not be mathematically feasible (for a detailed discussion on the choices of priors for Gaussian processes see [33]). We will elaborate on our assumptions and the prior choices we made in this appendix.

The GP approach has one main underlying assumption: continuity in $w(z)$. It is therefore rather different from the Principal Component Analysis (PCA) method which assumes a piecewise constant $w(z)$. The GP method is completely continuous and fully defined for all values of the domain and does not rely on its grid as break points or binning of any kind. The GP is fully defined in this case by its correlation function; we use the power exponential family: $K(z, z') = \kappa^2 \rho^{|z-z'|^\alpha}$. The parameters ($\rho$,$\kappa$,$\alpha$) are correlated with one another and do not have a simple interpretation. In our analysis we lock α to a certain value. A value of $\alpha = 2$ (Gaussian correlation) leads to very smooth (infinitely differentiable) results and does not allow for enough flexibility in capturing nontrivial behavior in $w(z)$ well. Thus, we have been using α=1 (exponential correlation) for this analysis, which provides a continuous GP (but non-differentiable everywhere). The other two parameters κ and ρ are variable and the best-fit values are dictated by the data.

Just as α influences the (small-scale) smoothness of the result, so does ρ. The smaller the value for the correlation length ρ, the more "features" will be picked up in $w(z)$ including unwanted noise. In other words, a very small correlation length can lead to overfitting. This can be avoided by choosing an informative prior for ρ. To elucidate this point further we investigate two different priors for ρ, a uniform, flat prior $\pi(\rho) \sim U(0, 1)$ and a more informative prior $\pi(\rho) \sim Beta(6, 1)$ which we also use in the main analysis. In Figure 10 (left column), we show

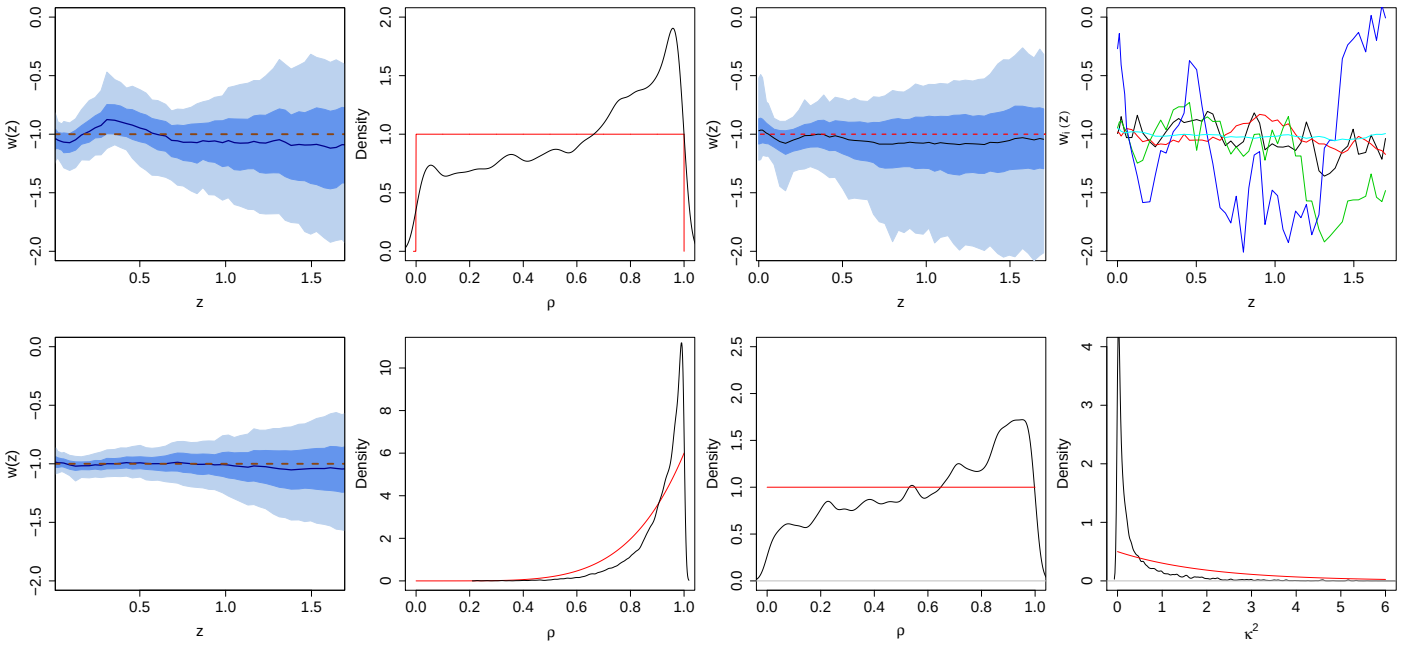

FIG. 10. Reconstruction results for $w(z)$ from 2298 simulated SNe measurements for different priors on ρ. Left column: $w(z)$ reconstruction with 68% and 95% confidence limits, right column: prior (red line) and posterior distribution (black line) for ρ. Upper row: flat prior on ρ, $\pi(\rho) \sim U(0,1)$. Right column: informative prior on ρ, $\pi(\rho) \sim Be(6,1)$.

FIG. 11. Reconstruction results following Figure 10, but now in addition to using a uniform prior for ρ we loosen the κ^2 prior: $\kappa^2 \sim G(1, 0.5)$, $\rho \sim U(0,1)$. The left upper panel shows the reconstruction result for $w(z)$ and the right upper panel shows some realizations (similar to Figure 2). The error bands in the prediction for $w(z)$ do increase in this case as expected. This case shows the most relaxed priors we study for this data set.

the differences for the reconstructed $w(z)$ for the two different priors (we use the simulated data for $w = const.$, 2298 SNe measurements). The uniform prior (upper row) produces a much noisier reconstruction result compared to the more informative prior (lower row). Also, the error bands increase due to the larger uncertainty in ρ. One important point to note in Figure 10 is that even for the flat prior, ρ shows a tendency toward high values – near unity in the posterior – justifying the more informative prior we use for the main analysis. In addition, the assumption of smoothness also suggests the more informative prior. The rather large values of ρ found in the final analysis indicate a rather smooth behavior of $w(z)$.

Finally, we also loosen the prior for κ^2 to demonstrate that our results are overall rather non-sensitive to the choices of the priors for the hyper-parameters. Our findings are summarized in Figure 11.

The upper left panel in Figure 11 shows the result for the reconstruction of $w(z)$. For κ^2 we choose a Gamma-distributed prior in this case ($\kappa^2 \sim G(1, 0.5)$) (lower right panel, prior in red). This prior does allow for a long positive tail for κ^2 but is not as strongly peaked close to zero as the inverse Gamma distribution. The posterior (in black) is sharply peaked at small values, in agreement with our more informative prior choice. The left lower panel shows the prior and posterior for ρ, a very similar result to Figure 10 (flat prior on ρ, inverse Gamma prior for κ^2). The error bands increase somewhat in this case but overall the reconstruction procedure works successfully. The upper right panel shows some of the realizations for $w(z)$. This figure demonstrates how much variation the GP model allows. Compared to Figure 2 it also shows that the choice of priors in this case drastically relaxes the assumption of smoothness on $w(z)$, the dark blue realization for example showing very large variations. Note that the peaks in the density distribution for κ^2 and ρ are similar as in the case of more informative priors. These results show nicely that our prior choices in the main paper are sensible and not overly restrictive. They also demonstrate that the correlation length is not a simple specifier of the variabilty across realizations, as previously discussed in Section IV.

ACKNOWLEDGMENTS

We would like to thank the Institute for Scalable Scientific Data Management for supporting this work. Part of this research was supported by the DOE under contract W-7405-ENG-36. UA, SH, KH, and DH acknowledge support from the LDRD program at Los Alamos National Laboratory. KH was supported in part by NASA.

SH and KH acknowledges the Aspen Center for Physics, where part of this work was carried out. We would like to thank Andreas Albrecht, Eric Linder, Adrian Pope, Martin White, and Michael Wood-Vasey for useful discussions.

[1] A.G. Riess *et al.* [Supernova Search Team Collaboration], Astron. J. **116**, 1009 (1998), arXiv:astro-ph/9805201.
[2] S. Perlmutter *et al.* [Supernova Cosmology Project Collaboration], Astrophys. J. **517**, 565 (1999), arXiv:astro-ph/9812133.
[3] M.J. Drinkwater *et al.*, Mon. Not. Roy. Astron. Soc. **401**, 1429 (2010), arXiv:0911.4246 [astro-ph.CO].
[4] D. Schlegel, M. White, and D. Eisenstein, arXiv:0902.4680 [astro-ph.CO]
[5] LSST Science Book, Version 2.0. [LSST Science Collaborations and LSST Project Collaboration], arXiv:0912.0201 [astro-ph.IM].
[6] D.J. Schlegel *et al.*, arXiv:1106.1706 [astro-ph.CO].
[7] N. Gehrels, arXiv:1008.4936 [astro-ph.CO].
[8] A. Refregier, A. Amara, T. D. Kitching, A. Rassat, R. Scaramella, J. Weller and f. t. E. Consortium, arXiv:1001.0061 [astro-ph.IM].
[9] C. Wetterich, Nucl. Phys. B **302**, 668 (1988); B. Ratra and P.J.E. Peebles, Phys. Rev. D **37**, 3406 (1988); P.J.E. Peebles and B. Ratra, Astrophys. J. **325**, L17 (1988); R.R. Caldwell, R. Dave and P.J. Steinhardt, Phys. Rev. Lett. **80**, 1582 (1998) .
[10] M. Chevallier and D. Polarski, Int. J. Mod. Phys. D **10**, 213 (2001), arXiv:gr-qc/0009008.
[11] E.V. Linder, Phys. Rev. Lett. **90**, 091301 (2003), arXiv:astro-ph/0208512.
[12] M. Hicken *et al.*, Astrophys. J. **700**, 1097 (2009), arXiv:0901.4804 [astro-ph.CO].
[13] R. Amanullah *et al.*, Astrophys. J. **716**, 712 (2010), arXiv:1004.1711 [astro-ph.CO].
[14] M. Sullivan *et al.*, arXiv:1104.1444 [astro-ph.CO].
[15] A.R. Cooray and D. Huterer, Astrophys. J. **513**, L95 (1999), arXiv:astro-ph/9901097; I. Maor, R. Brustein and P.J. Steinhardt, Phys. Rev. Lett. **86**, 6 (2001) [Erratum-ibid. **87**, 049901 (2001)], arXiv:astro-ph/0007297; J. Weller and A.J. Albrecht, Phys. Rev. Lett. **86**, 1939 (2001), arXiv:astro-ph/0008314.
[16] R.A. Daly and S.G. Djorgovski, Astrophys. J. **597**, 9 (2003), arXiv:astro-ph/0305197; D. Huterer and A. Cooray, Phys. Rev. D **71**, 023506 (2005), arXiv:astro-ph/0404062; C. Zunckel and R. Trotta, Mon. Not. Roy. Astron. Soc. **380**, 865 (2007), arXiv:astro-ph/0702695; C. Clarkson and C. Zunckel, Phys. Rev. Lett. **104**, 211301 (2010), arXiv:1002.5004 [astro-ph.CO].
[17] F. Simpson and S.L. Bridle, Phys.Rev. D, **73**, 083001 (2006), arXiv:astro-ph/0602213.
[18] T. Holsclaw, U. Alam, B. Sanso, H. Lee, K. Heitmann, S. Habib, and D. Higdon, Phys. Rev. D **82**, 103502 (2010), arXiv:1009.5443 [astro-ph.CO].
[19] T. Holsclaw, U. Alam, B. Sanso, H. Lee, K. Heitmann, S. Habib, and D. Higdon, Phys. Rev. Lett. **105**, 241302 (2010), arXiv:1011.3079 [astro-ph.CO].
[20] E. Komatsu *et al.* [WMAP Collaboration], Astrophys. J. Suppl. **192**, 18 (2011), arXiv:1001.4538 [astro-ph.CO].
[21] J.R. Bond, G. Efstathiou, and M. Tegmark, Mon. Not. Roy. Astron. Soc. **291**, L33 (1997), arXiv:astro-ph/9702100.
[22] Y. Wang and P. Mukherjee, Phys. Rev. D **76**, 103533 (2007), arXiv:astro-ph/0703780.
[23] O. Elgaroy and T. Multamaki, Astron. & Astrophys. **471**, 65 (2007), arXiv:astro-ph/0702343.
[24] P.S. Corasaniti and A. Melchiorri, Phys. Rev. D **77**, 103507 (2008), arXiv:0711.4119 [astro-ph].
[25] S. Banerjee, B.P. Carlin, and A.E. Gelfand, *Hierarchical Modeling and Analysis for Spatial Data*, New York: Chapman and Hall (2004); C.E. Rasmussen and K.I. Williams, *Gaussian Processes for Machine Learning*, Boston: MIT Press (2006).
[26] D. Gamerman and H.F. Lopes, *Markov Chain Monte Carlo: Stochastic Simulation for Bayesian Inference*, New York: Chapman and Hall (2006).
[27] A. Gelman, B. Carlin, H. Stern, and D. Rubin, *Bayesian Data Analysis*, New York: Chapman and Hall (2004).
[28] M. Kowalski et al., Astrophys. J. **686**, 749 (2008).
[29] W.J. Percival *et al.*, Mon. Not. Roy. Astron. Soc. **401**, 2148 (2010), arXiv:arXiv:0907.1660 [astro-ph].
[30] H-J. Seo and D. J. Eisenstein, Astrophys. J **665**, 14 (2007), astro-ph/0701079.
[31] D. J. Eisenstein, H-J. Seo, and M. White, Astrophys. J. **664**, 660 (2007), astro-ph/0604361.
[32] C. Escamilla-Rivera, R. Lazkoz, V. Salzano and I. Sendra, arXiv:1103.2386 [astro-ph.CO].
[33] J.O. Berger, V. de Oliveira, and B. Sansó, Journal of the American Statistical Association, **96**, 1361 (2001).